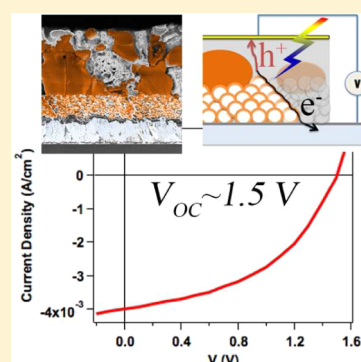Letter

Chloride Inclusion and Hole Transport Material Doping to Improve Methyl Ammonium Lead Bromide Perovskite-Based High Open-Circuit Voltage Solar Cells

Eran Edri,[†] Saar Kirmayer,[†] Michael Kulbak, Gary Hodes,* and David Cahen*

Department of Materials & Interfaces, Weizmann Institute of Science, Rehovot 76100, Israel

ABSTRACT: Low-cost solar cells with high V_{OC}, relatively small ($E_G - qV_{OC}$), and high qV_{OC}/E_G ratio, where E_G is the absorber band gap, are long sought after, especially for use in tandem cells or other systems with spectral splitting. We report a significant improvement in $CH_3NH_3PbBr_3$-based cells, using $CH_3NH_3PbBr_{3-x}Cl_x$, with $E_G = 2.3$ eV, as the absorber in a mesoporous p−i−n device configuration. By p-doping an organic hole transport material with a deep HOMO level and wide band gap to reduce recombination, the cell's V_{OC} increased to 1.5 V, a 0.2 V increase from our earlier results with the pristine Br analogue with an identical band gap. At the same time, in the most efficient devices, the current density increased from ~1 to ~4 mA/cm².

SECTION: Energy Conversion and Storage; Energy and Charge Transport

Inexpensive solar cells that use only the high-energy part of the solar spectrum and yield high open-circuit voltage, V_{OC}, are missing from the palette of photovoltaic technologies. They are needed to make more efficient use of the high-energy part of the solar spectrum and can serve as the front cell in tandem cells or in a general spectral splitting system. Such a cell should have an absorber with a suitable band gap, E_G, and the alignment of the energy bands/levels of the cell components should minimize energy losses after electron−hole pair photogeneration, including slow recombination kinetics − efficient extraction rates. Practically, this is expressed not only in high qV_{OC}/E_G and J_{SC}/J_{SC}^{MAX} (J_{SC}: short-circuit current; J_{SC}^{MAX}: theoretically maximal J_{SC} for the specific E_G of the material) but also in a high fill factor. Because this type of solar cell uses only part of the spectrum, its overall efficiency is limited by its J_{SC}^{MAX}.[1]

Currently, GaInP photovoltaic devices are used as top cell in inorganic tandem systems, with cell s $V_{OC} \approx 1.45$ V and a very high $qV_{OC}/E_G \approx 0.8$. However, these devices are expensive, and therefore, although they increase the overall efficiency of a tandem system, they also increase the cost per watt. A low-cost way for possible large-scale cell fabrication is through low-temperature solution methods. Solution-made high V_{OC} devices were reported using all-organic cells, with the AM1.5 V_{OC} reaching 1.5 V although with low $J_{SC} < 2$ mA/cm².[2,3] In the last couple of years, a "new" material system that appears to suit these requirements has emerged.[4−6] Methyl ammonium lead halide perovskite solar cells have shown a remarkable power conversion efficiency (PCE) and qV_{OC}/E_G (and $E_G − qV_{OC}$) values for such a recent technology, reaching an appreciable $qV_{OC}/E_G \approx 0.7$, with $E_G = 1.55$ eV for $CH_3NH_3PbI_{3-x}Cl_x$[7] and $qV_{OC}/E_G \approx 0.67$ for $CH_3NH_3PbI_3$ ($E_G − qV_{OC} \approx 0.45$ and 0.5

eV, respectively),[8] already comparable with more "mature" technologies. Extrapolating this high figure to a material of higher band gap, one with $E_G = 1.9−2.3$ eV (and carefully selecting the selective contact materials), we can expect a photovoltaic device with $V_{OC} \approx 1.3−1.6$ V (or if the same loss mechanisms are considered as those in the iodine devices, we can expect 1.5−1.9 V). Indeed, devices using the higher band gap analogue, $CH_3NH_3PbBr_3$ ($E_G = 2.3$ eV), were devised,[9] and an increase in V_{OC} was observed with increasing E_G, which resulted in a V_{OC} of 1.13 V. Earlier, we showed that a high V_{OC} device (reaching 1.3 V) can be obtained with cells based on $CH_3NH_3PbBr_3$ and perylene diimide (PDI) as hole transport material (HTM).[10] However, the qV_{OC}/E_G ratio was only ~55% (and $E_G − qV_{OC} \approx 1$ eV), and current densities were limited to 1−1.5 mA/cm². We argued there that one of the limitations on the current densities was the low light absorption in the nonuniform film and losses due to absorption in the HTM.

Recently, it was shown that the effective diffusion lengths for electrons and holes in $CH_3NH_3PbI_{3-x}Cl_x$ alone[12] or in a working cell structure[11] are 1.9 and 1.2 μm, respectively, and direct evidence was given that the cell works as a p−i−n photovoltaic device.[11] At the same time, for reasons that are not yet clear, $CH_3NH_3PbI_3$ shows a comparable effective diffusion length for holes but a shorter one for electrons,[11−13] so that a mesoporous electron conducting matrix is needed to make $CH_3NH_3PbI_3$-based devices efficient. Such a cell resembles an
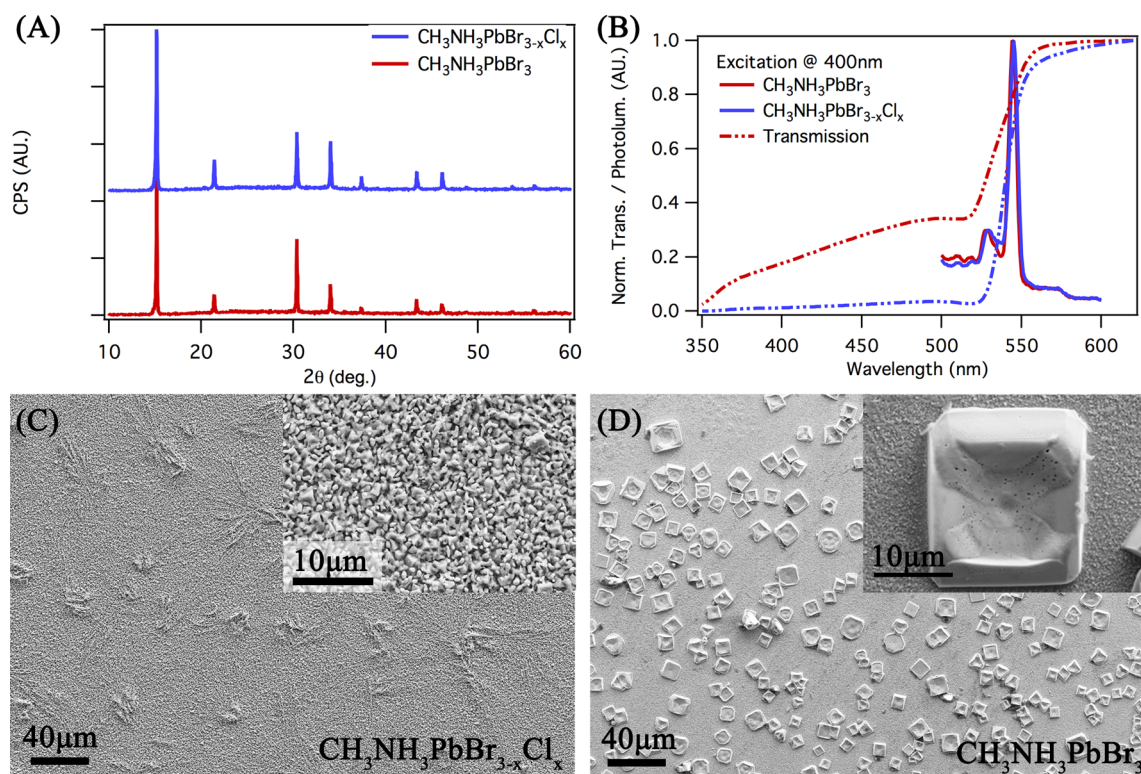
Figure 1. X-ray diffractograms of spin-coated films of $CH_3NH_3PbBr_3$ and $CH_3NH_3PbBr_{3-x}Cl_x$ (A) and the corresponding transmission (dash−dot) and photoluminescence (solid lines) spectra of the same films (B). Plan view SEM images of $CH_3NH_3PbBr_{3-x}Cl_x$ (C) and $CH_3NH_3PbBr_3$ (D), both spin-coated on FTO.
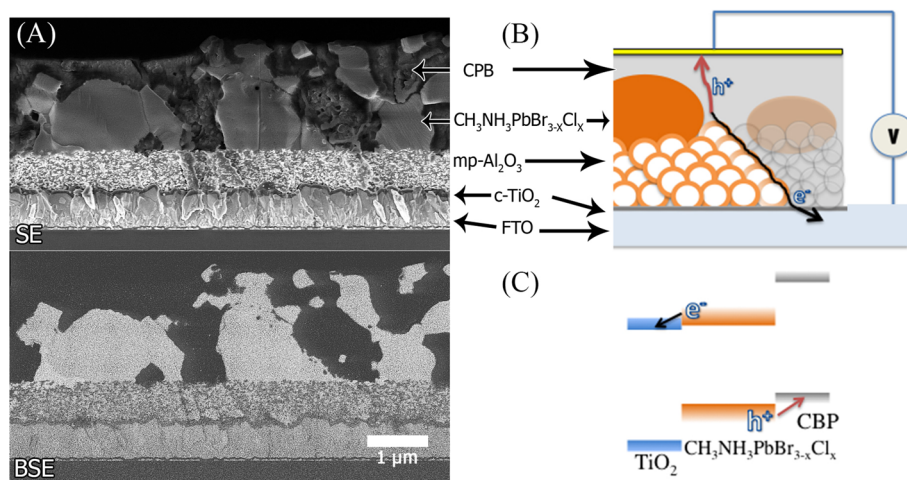

Figure 2. Cross-sectional SEM image of a cell (A) with secondary (top) and backscattered (bottom) electron detectors. (B) Schematic design of a cell (not to scale), showing the different parts of the cell. (C) Schematic energy alignment diagram in the device (B), showing its suggested operation.

extremely thin absorber (ETA) one and results in lower V_{OC} values than those with the absorber, prepared with both Cl and I precursors. Therefore, the motivation to make a Br analogue of $CH_3NH_3PbI_{3-x}Cl_x$ is clear, although previously,[10] the use of mesoporous TiO_2 was not advantageous for the device performance and resulted in lower V_{OC}, which suggests that $CH_3NH_3PbBr_3$ does not necessarily have a relatively short diffusion length for electrons as $CH_3NH_3PbI_3$ does. Nonetheless, as we show here, the effect of Cl in the precursor solution of the absorber on the device performance is profound, even if

also here the underlying physicochemical reasons are not yet understood.

On the HTM side, although PDI showed good hole mobility,[14] one of its limitations is that it is difficult to dope p-type, which limits its conductivity and, thus, the J_{SC} and fill factor of PDI-based cells. Furthermore, we found recently that in the device form, the PDI HOMO−LUMO states align poorly with the $CH_3NH_3PbBr_3$ valence and conduction band edges, limiting its efficacy as a selective contact for holes.[15] In contrast, 4,4′-bis(N-carbazolyl)-1,1′-biphenyl (CBP) is a HTM that could meet the requirements that PDI lacks, that is, with its
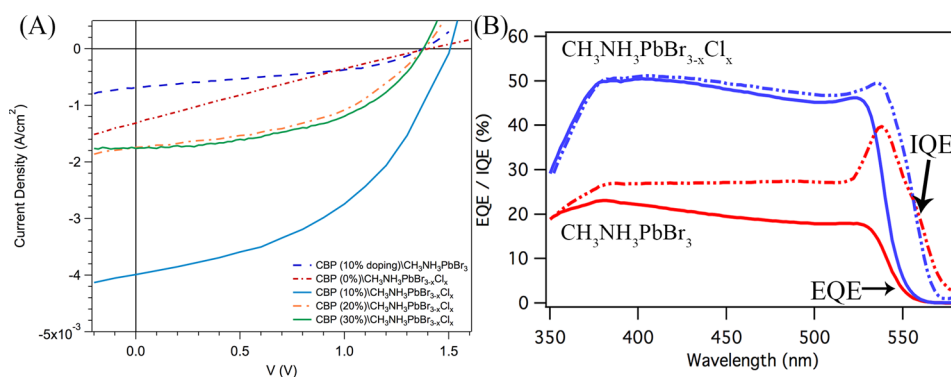
Figure 3. (A) Current−voltage (I−V) curves of devices with $CH_3NH_3PbBr_3$ (blue dashed line) and $CH_3NH_3PbBr_{3−x}Cl_x$ (blue solid line) with the CBP hole conductor doped 10 mol % with LiTFSi and devices with 0 (red short dash−dot), 20 (orange dash−dot), and 30% doping (green solid) at 100 W/cm². (B) External and internal quantum efficiency (EQE and IQE, respectively) of devices with $CH_3NH_3PbBr_3$ (red) and $CH_3NH_3PbBr_{3−x}Cl_x$ (blue) with CBP doped with 10 mol % LiTFSi. I−V scans were taken at a rate of 1 V/sec for all devices. All of the scans shown are from reverse to forward bias.

high band gap and deeper HOMO level, it is more likely to be selective toward hole injection (i.e., a better electron blocker), give higher V_{OC}, and be chemically p-doped to make it more conductive.[16]

Here, we show, for the first time, that by using the Br analogue of $CH_3NH_3PbI_{3−x}Cl_x$, that is, $CH_3NH_3PbBr_{3−x}Cl_x$, together with p-doped CBP, devices with 200 mV higher V_{OC} and with ∼3 times higher currents than those reported earlier can be made.

$CH_3NH_3PbBr_{3−x}Cl_x$ and $CH_3NH_3PbBr_3$ thin films were prepared by spin-casting a solution made of a 3:1 $CH_3NH_3Br/PbCl_2$ mol ratio for $CH_3NH_3PbBr_{3−x}Cl_x$ or a 1:1 mol ratio of a $CH_3NH_3Br/PbBr_2$ solution for $CH_3NH_3PbBr_3$ and forming the film by heating the substrate (see the Experimental Methods section for more details). X-ray diffractograms of $CH_3NH_3PbBr_{3−x}Cl_x$ and $CH_3NH_3PbBr_3$ thin films on glass substrates are shown in Figure 1A alongside the optical transmission and photoluminescence spectra of the films (Figure 1B).

Both materials exhibit similar band gap values and X-ray diffractograms. In addition, $CH_3NH_3PbBr_3$ shows higher transmission in the 350−525 nm (∼3.5 to ∼2.4 eV) range than does $CH_3NH_3PbBr_{3−x}Cl_x$, which we attribute to the film nonuniformity, as can be seen in Figure 1C and D. The presence of $Cl^−$ and/or an excess of $CH_3NH_3^+$ in the solution results in smaller crystallites (although still in the few 100s of nm range), which cover the surface more densely than without this excess and lead to better light absorption. As is the case for the better-studied iodide analogue, no Cl is detected in the film by energy dispersive spectroscopy (EDS). As X-ray photoelectron spectroscopy shows a few % Cl in the material, we conclude that, on average, Cl is present in the film below the EDS detection limit, possibly concentrated at/near the surface. This explains the difference from previous studies[17] that have shown a continuous increase in the optical band gap with the addition of chlorine, along with a shift of X-ray diffraction peaks; the exact amount and distribution of Cl and its correlation with the film and crystal structure and device performance are matters of ongoing research.

In Figure 2, a SEM cross-sectional image of a $CH_3NH_3PbBr_{3−x}Cl_x$-based device with a suggested diagram of the energy alignment in the device is shown. The backscattered electron image, sensitive to the atomic number of the elements, shows the complexity of the morphology in these films.

Adding Cl to the $CH_3NH_3PbBr_3$ to yield $CH_3NH_3PbBr_{3−x}Cl_x$ increases the open-circuit voltage, fill factor, and, especially, the current density (Figure 3A). A V_{OC} of 1.57 V was measured directly (i.e., before cell heating occurred), while in a I−V sweep, V_{OC} = 1.5 eV and J_{SC} = 4 mA/cm² ($J_{SC}^{MAX} \approx 9$ mA/cm², that is, $J_{SC}/J_{SC}^{MAX} \approx 0.45$), resulting in ∼2.5% PCE for the best $CH_3NH_3PbBr_{3−x}Cl_x$-based cell. The difference between the 1.57 V direct measurement and 1.5 V from the I−V measurement is due mainly to the heating by the light source in the latter (much slower) measurement.

The external and internal quantum efficiencies (EQE and IQE, respectively) of $CH_3NH_3PbBr_3$- and $CH_3NH_3PbBr_{3−x}Cl_x$-based devices are shown in Figure 3B, showing EQE values reaching 50% for $CH_3NH_3PbBr_{3−x}Cl_x$-based cells. Similar values of IQE were calculated, demonstrating that recombination in these devices is not very high. The situation is different for $CH_3NH_3PbBr_3$-based devices, where a difference between the EQE and IQE spectra is observed, increasing from a few to ∼10% toward the longer wavelength part of the spectrum due to a reduction in the EQE in this region. The nearly constant IQE indicates that charges, photogenerated away from the FTO, are extracted as efficiently as charges close to the FTO; however, the lower absorption in the $CH_3NH_3PbBr_3$ film toward the longer wavelengths results in a lower EQE in that region.

As noted before,[18] p-type doping of the organic HTM can be obtained by oxygen incorporation in the layer. Lithium bis(trifluoromethanesulfonyl)imide (LITFSI) is suggested to have this effect in other organic hole conductors and was used to improve the HTM conductivity.[18] As shown in Figure 3, without doping, a device with a ∼ 25% fill factor is obtained, and the current is limited. Upon doping, the conductivity increases, and the overall performance of the device improves, especially the fill factor and J_{SC}. Further increasing the dopant concentration in the HTM reduces device performance, possibly due to opposing effects caused by the Li additive, as observed and described before.[19] The photovoltaic performance of the devices is summarized in Table 1.

To conclude, we have shown that by improved selection of materials, the V_{OC} of devices can be increased, realizing a qV_{OC}/E_G close to 0.7 ($E_G − qV_{OC} \approx 0.73$ V for the direct measurement), with a high band gap absorber in a (mostly) solution-made device. Currently, we ascribe this improvement to better surface coverage of the perovskite with Cl than that

Table 1. Summary of the Photovoltaic Parameters

device	V_{OC} (V)	J_{SC} (mA·cm^{-2})	fill factor (%)	PCE (%)
CH$_3$NH$_3$PbBr$_3$/ CBP (10%)[a]	1.38	0.7	40	0.37
CH$_3$NH$_3$PbBr$_{3-x}$Cl$_x$/CBP (0%)	1.40	1.3	24	0.44
CH$_3$NH$_3$PbBr$_{3-x}$Cl$_x$/CBP (10%)[b]	1.50	4.0	46	2.70
CH$_3$NH$_3$PbBr$_{3-x}$Cl$_x$/CBP (20%)	1.35	1.8	34	0.81
CH$_3$NH$_3$PbBr$_{3-x}$Cl$_x$/CBP (30%)	1.38	1.9	40	1.05

[a]The number in parentheses is the molar doping ratio of LiTFSi with respect to CBP. [b]The results were successfully reproduced in three separate experiments, by two experimentalists. A V_{OC} of 1.42−1.5 and a J_{SC} of 2.5−4 mA·cm^{-2} were obtained

without, which results in increased light absorption, and to the HTM that is more selective toward charge injection. Doping the HTM further reduces the series resistance and improves device performance. Further improvements should be possible by improving the absorber surface coverage and further optimization of the properties of the different layers in the device.

■ EXPERIMENTAL METHODS

Device Fabrication. F-doped tin oxide (FTO) transparent conducting substrates (Pilkington TEC15) were cut and cleaned by sequential 15 min sonication in warm aqueous alconox solution, deionized water, acetone, and ethanol, followed by drying in a N$_2$ stream. A compact ∼100 nm thin TiO$_2$ was then applied to the clean substrate by spray pyrolysis of a 20 mM titanium diisopropoxide bis(acetylacetonate) solution in isopropanol using air as the carrier gas on a hot plate set to 350 °C, followed by annealing at 500 °C for 1 h in air. A mesoporous alumina layer was applied by adapting the procedure reported in ref 4 to make the paste, followed by diluting in ethanol to the needed viscosity and spin-coating at 3000 rpm for 45 s.

A CH$_3$NH$_3$PbBr$_3$ solution was prepared as described elsewhere.[6] In short, CH$_3$NH$_3$Br was prepared by mixing methyl amine (40% in methanol) with hydrobromic acid (48% in water; CAUTION: exothermic reaction) in a 1:1 molar ratio in a 100 mL flask under continuous stirring at 0 °C for 2 h. CH$_3$NH$_3$Br was then crystallized by removing the solvent in a rotary evaporator, washing three times in diethyl ether for 30 min, and filtering the precipitate. The material, in the form of white crystals, was dried overnight in vacuo at 60 °C. It was then kept in a dark, dry environment until further use. A 40 wt % solution of CH$_3$NH$_3$PbBr$_3$ was prepared by mixing PbBr$_2$ and CH$_3$NH$_3$Br in an equimolar ratio in anhydrous dimethyl formamide (DMF). A 40 wt % solution of CH$_3$NH$_3$PbBr$_{3-x}$Cl$_x$ was prepared by mixing PbCl$_2$ and CH$_3$NH$_3$Br in a 3:1 mol ratio in DMF. To coat the substrate, the solution was spin-coated in two stages, 5 s at 500 rpm and then at 1500 rpm for 30 s. The substrate was then heated on a hot plate set at 150 °C for 60 min (CH$_3$NH$_3$PbBr$_{3-x}$Cl$_x$) or 120 °C for 45 min (CH$_3$NH$_3$PbBr$_3$), after which the substrate turned orange in color. All procedures were carried out in an ambient atmosphere.

To finish the device fabrication, 150 μL of a hot (ca. 60 °C) hole conductor solution (84 mg of CBP in 1 mL of chlorobenzene, mixed with 7 μL of *tert*-butylpyridine and 15

μL of 170 mg/mL LiTFSI, bis(trifluoromethane)sulfonamide (in acetonitrile)), was applied by spin-coating 5 s at 500 rpm and then at 1500 rpm for 30 s. The samples were left overnight in the dark in dry air before 100 nm gold contacts were thermally evaporated on the back through a shadow mask with 0.24 cm^2 rectangular holes.

Device Characterization. The $J-V$ characteristics were measured with a Keithley 2400-LV SourceMeter and controlled with a Labview-based, in-house written program. A solar simulator (ScienceTech SF-150) equipped with a 1.5AM filter and calibrated with a Si solar cell IXOLAR High Efficiency SolarBIT (IXYS XOB17-04x3) was used for illumination. The devices were characterized through a 0.16 cm^2 mask.

Transmission and reflection of films were measured using Jasco V-570 equipped with an integrating sphere. Transmission was corrected for reflection by using $T_{corr} = T/(1 - R)$.

The EQE and IQE were measured with a Thermo Oriel monochromator with the light chopped at 10 Hz. The current was measured using an Oriel Merlin and TTI PDA-700 photodiode amplifier. The EQE was calculated by referencing to the spectral response of a Si photodiode with a known EQE. The IQE was calculated by taking the ratio of EQE to the corrected and normalized transmission.

XRD measurements were conducted on a Rigaku ULTIMA III operated with a Cu anode at 40 kV and 40 mA. The measurements were taken using a Bragg−Brentano configuration through a 10 mm slit, a convergence Soller 5° slit and a Ni filter.

Photoluminescence was measured on a Varian Cary Eclipse, using a 2.5 nm excitation slit and 5 nm emission slit. The excitation wavelength was 400 nm, and an emission band filter of 410−900 nm was used to prevent the excitation beam from reaching the detector.

For morphology studies, a Leo Ultra 55 scanning electron microscope was used, in most cases using 2 kV accelerating voltage.

■ AUTHOR INFORMATION

Corresponding Authors
*E-mail: david.cahen@weizmann.ac.il (D.C.).
*E-mail: gary.hodes@weizmann.ac.il (G.H.).

Author Contributions
[†]E.E. and S.K. contributed equally.

Notes
The authors declare no competing financial interest.

■ ACKNOWLEDGMENTS

■ REFERENCES

(1) Nayak, P. K.; Cahen, D. Updated Assessment of Possibilities and Limits for Solar Cells. *Adv. Mater.* **2013**, DOI: 10.1002/adma.201304620.
(2) Egbe, D. A. M.; Kietzke, T.; Carbonnier, B.; Mühlbacher, D.; Hörhold, H.-H.; Neher, D.; Pakula, T. Synthesis, Characterization, and Photophysical, Electrochemical, Electroluminescent, and Photovoltaic Properties of Yne-Containing CN−PPVs. *Macromolecules* **2004**, 37, 8863−8873.

(3) Kietzke, T.; Egbe, D. A. M.; Hörhold, H.-H.; Neher, D. Comparative Study of M3EH−PPV-Based Bilayer Photovoltaic Devices. *Macromolecules* **2006**, *39*, 4018−4022.

(4) Lee, M. M.; Teuscher, J.; Miyasaka, T.; Murakami, T. N.; Snaith, H. J. Efficient Hybrid Solar Cells Based on Meso-Superstructured Organometal Halide Perovskites. *Science* **2012**, *338*, 643−647.

(5) Kim, H.-S.; Lee, C.-R.; Im, J.-H.; Lee, K.-B.; Moehl, T.; Marchioro, A.; Moon, S.-J.; Humphry-Baker, R.; Yum, J.-H.; Moser, J. E.; et al. Lead Iodide Perovskite Sensitized All-Solid-State Submicron Thin Film Mesoscopic Solar Cell with Efficiency Exceeding 9%. *Sci. Rep.* **2012**, *2*, 591 DOI: 10.1038/srep00591.

(6) Kojima, A.; Teshima, K.; Shirai, Y.; Miyasaka, T. Organometal Halide Perovskites as Visible-Light Sensitizers for Photovoltaic Cells. *J. Am. Chem. Soc.* **2009**, *131*, 6050−6051.

(7) Snaith, H. J. Perovskites: The Emergence of a New Era for Low-Cost, High-Efficiency Solar Cells. *J. Phys. Chem. Lett.* **2013**, 3623−3630.

(8) Malinkiewicz, O.; Yella, A.; Lee, Y. H.; Espallargas, G. M.; Graetzel, M.; Nazeeruddin, M. K.; Bolink, H. J. Perovskite Solar Cells Employing Organic Charge-Transport Layers. *Nat. Photonics* **2013**, DOI: 10.1038/NPHOTON.2013.341.

(9) Noh, J. H.; Im, S. H.; Heo, J. H.; Mandal, T. N.; Seok, S. I. Chemical Management for Colorful, Efficient, and Stable Inorganic−Organic Hybrid Nanostructured Solar Cells. *Nano Lett.* **2013**, *13*, 1764−1769.

(10) Edri, E.; Kirmayer, S.; Cahen, D.; Hodes, G. High Open-Circuit Voltage Solar Cells Based on Organic−Inorganic Lead Bromide Perovskite. *J. Phys. Chem. Lett.* **2013**, *4*, 897−902.

(11) Edri, E.; Kirmayer, S.; Mukhopadhyay, S.; Gartsman, K.; Hodes, G.; Cahen, D. How do $CH_3NH_3PbI_{3−x}Clx$ Solar Cells Work? *Rump Session for Organo-metal Halide Perovskite-Based Solar Cells*; 2013 MRS Fall Meeting & Exhibit, Boston, MA, Dec. 1−6, 2013.

(12) Stranks, S. D.; Eperon, G. E.; Grancini, G.; Menelaou, C.; Alcocer, M. J.; Leijtens, T.; Herz, L. M.; Petrozza, A.; Snaith, H. J. Electron−Hole Diffusion Lengths Exceeding 1 Micrometer in an Organometal Trihalide Perovskite Absorber. *Science* **2013**, *342*, 341−344.

(13) Xing, G.; Mathews, N.; Sun, S.; Lim, S. S.; Lam, Y. M.; Grätzel, M.; Mhaisalkar, S.; Sum, T. C. Long-Range Balanced Electron- and Hole-Transport Lengths in Organic−Inorganic CH3NH3PbI3. *Science* **2013**, *342*, 344−347.

(14) Delgado, M. C. R.; Kim, E.-G.; Filho, D. A.; da, S.; Bredas, J.-L. Tuning the Charge-Transport Parameters of Perylene Diimide Single Crystals via End and/or Core Functionalization: A Density Functional Theory Investigation. *J. Am. Chem. Soc.* **2010**, *132*, 3375−3387.

(15) Schulz, P.; Kirmayer, S.; Edri, E.; Hodes, G.; Cahen, D.; Kahn, A. Interface Energetics of Organo-Metal Halide Perovskites in Hybrid Photovoltaics. *Rump Session for Organo-metal Halide Perovskite-Based Solar Cells*; 2013 MRS Fall Meeting & Exhibit, Boston, MA, Dec. 1−6, 2013.

(16) Kröger, M.; Hamwi, S.; Meyer, J.; Riedl, T.; Kowalsky, W.; Kahn, A. P-Type Doping of Organic Wide Band Gap Materials by Transition Metal Oxides: A Case-Study on Molybdenum Trioxide. *Org. Electron.* **2009**, *10*, 932−938.

(17) Kitazawa, N.; Watanabe, Y.; Nakamura, Y. Optical Properties of $CH_3NH_3PbX_3$ (X = Halogen) and Their Mixed-Halide Crystals. *J. Mater. Sci.* **2002**, *37*, 3585−3587.

(18) Nayak, P. K.; Rosenberg, R.; Barnea-Nehoshtan, L.; Cahen, D. O_2 and Organic Semiconductors: Electronic Effects. *Org. Electron.* **2013**, *14*, 966−972.

(19) Abate, A.; Leijtens, T.; Pathak, S.; Teuscher, J.; Avolio, R.; Errico, M. E.; Kirkpatrik, J.; Ball, J. M.; Docampo, P.; McPherson, I. Lithium Salts as "Redox Active" P-Type Dopants for Organic Semiconductors and Their Impact in Solid-State Dye-Sensitized Solar Cells. *Phys. Chem. Chem. Phys.* **2013**, *15*, 2572−2579.